# Key feature of the catalytic cycle of TNF-{alpha} converting enzyme involves communication between distal protein sites and the enzyme catalytic core

Ariel Solomon, Barak Akabayov, Anatoly Frenkel, Marcos E. Milla, and Irit Sagi

**This information is current as of March 2007.**

| | |
|---|---|
| **Supplementary Material** | Supplementary material can be found at: <br> www.pnas.org/cgi/content/full/0700066104/DC1 <br><br> This article has been cited by other articles: <br> www.pnas.org#otherarticles |
| **E-mail Alerts** | Receive free email alerts when new articles cite this article - sign up in the box at the top right corner of the article or click here. |
| **Rights & Permissions** | To reproduce this article in part (figures, tables) or in entirety, see: <br> www.pnas.org/misc/rightperm.shtml |
| **Reprints** | To order reprints, see: <br> www.pnas.org/misc/reprints.shtml |

Notes:

# Key feature of the catalytic cycle of TNF-α converting enzyme involves communication between distal protein sites and the enzyme catalytic core

Ariel Solomon*, Barak Akabayov*, Anatoly Frenkel†, Marcos E. Milla‡, and Irit Sagi*§

*Department of Structural Biology, Weizmann Institute of Science, Rehovot 76100, Israel; ‡Department of Biochemical Pharmacology, Roche Pharmaceuticals, Palo Alto, CA 94304; and †Department of Physics, Yeshiva University, New York, NY 10033

Despite their key roles in many normal and pathological processes, the molecular details by which zinc-dependent proteases hydrolyze their physiological substrates remain elusive. Advanced theoretical analyses have suggested reaction models for which there is limited and controversial experimental evidence. Here we report the structure, chemistry and lifetime of transient metal–protein reaction intermediates evolving during the substrate turnover reaction of a metalloproteinase, the tumor necrosis factor-α converting enzyme (TACE). TACE controls multiple signal transduction pathways through the proteolytic release of the extracellular domain of a host of membrane-bound factors and receptors. Using stopped-flow x-ray spectroscopy methods together with transient kinetic analyses, we demonstrate that TACE's catalytic zinc ion undergoes dynamic charge transitions before substrate binding to the metal ion. This indicates previously undescribed communication pathways taking place between distal protein sites and the enzyme catalytic core. The observed charge transitions are synchronized with distinct phases in the reaction kinetics and changes in metal coordination chemistry mediated by the binding of the peptide substrate to the catalytic metal ion and product release. Here we report key local charge transitions critical for proteolysis as well as long sought evidence for the proposed reaction model of peptide hydrolysis. This study provides a general approach for gaining critical insights into the molecular basis of substrate recognition and turnover by zinc metalloproteinases that may be used for drug design.

dynamics | matrix metalloproteinases | proteolysis | x-ray absorption | stopped flow

Zinc-dependent metalloproteinases comprise a large superfamily of enzymes possessing key biological roles. These enzymes use zinc (Fig. 1*a*) to catalyze the hydrolysis of peptide bonds in a wide variety of substrates in both normal and pathological processes (1, 2). Over the last five decades, substantial efforts have been aimed at understanding the molecular basis by which the catalytic zinc machinery executes such enzymatic reactions (3, 4). Protein crystallography, proteomic, and theoretical studies have been instrumental in proposing reaction mechanisms (3, 5, 6). However, the molecular details that link the catalytic chemistry to key kinetic, electronic, and structural events have remained elusive because of the difficulties associated with probing time-dependent structure–function aspects of such reactions in the presence of peptide substrates.

Here we used a strategy based on dynamic structural spectroscopy to elucidate in detail the molecular mechanisms at work during substrate turnover by TACE. TACE is a disintegrin and metalloproteinase family member (also known as ADAM 17) with key roles in the regulation of the proteolytic release of cytokines, chemokines, growth factors, and receptors from cellular membranes (a process known as ectodomain shedding) (7). We have used stopped-flow freeze-quench x-ray absorption spectroscopy (XAS) in conjunction with transient kinetic studies to probe changes in the structure and reactivity of the catalytic zinc–protein complex in real-time. We have quantified the structure, electronics, and lifetime of the evolving zinc–protein reaction intermediates during the peptide hydrolysis reaction. Thus, we provide a correlation between the distinct kinetic phases involved in the proteolytic reaction and key structural and electronic intermediates evolving at TACE's active site.

## Transient Kinetic Analysis

To determine the kinetic phases of the substrate cleavage reaction and their lifetimes, we conducted steady-state and pre-steady-state kinetic analyses of TACE during peptide hydrolysis, using a fluorogenic substrate that spans the cleavage site of precursor TNF-α (QF45: Mca-SPLAQAVRSSSRK-(Dnp)-NH₂ (8) (see Fig. 1*b*). Peptide hydrolysis characterization was done under conditions that were independent of reactant concentrations to isolate the peptide hydrolysis event from substrate/enzyme association. Specifically, TACE proteolysis was studied by increasing substrate/enzyme molar ratios until no change in rate was observed. Fig. 1*b* describes the peptide hydrolysis reaction under multiple turnover conditions in which different kinetic phases are resolved. Three distinct kinetic phases were observed (Fig. 1*b*): (*i*) A lag phase of ≈34 ms (the dead time of the stopped flow instrument is 2.1 ms); (*ii*) a burst phase from 34 to 105 ms; and (*iii*) a steady-state phase extending beyond 105 ms. The relatively high amplitude ratios of the pre-steady-state burst and steady-state phases implies that the rate limiting step for TACE substrate cleavage is product release (9). The nonlinear curve fitting analysis of kinetic traces supports this point. The rate of the pre-steady-state burst, $k_{obs}$ of 64 s$^{-1}$ at 37°C, indicates that the actual catalysis is fast and that the reaction limiting step is the substrate dissociation.

## Correlation of Turnover Kinetics with Structural Changes

We have used stopped-flow freeze-quench XAS procedures (10) to structurally characterize TACE's catalytic site during substrate turnover. XAS provides local structural and electronic information about the nearest coordination environment surrounding the catalytic metal ion within the active site of a metalloprotein in solution (for detailed review, see Strange and Hasnain; ref. 11). Time-dependent XAS provides insight into the lifetimes and local atomic structures of metal–protein complexes during enzymatic reactions on millisecond to minute time scales (10) [see supporting information (SI) *Text* for details]. This type

BIOPHYSICS

a



His415
His409
His405
H₂O
Glu406

b



**Fig. 1.** Zinc-dependent peptide hydrolysis. (*a*) Schematic depiction of the catalytic zinc site of TACE. This model represents the resting active state of the enzyme. The optimized structural model was produced from the crystallographic coordinates of inhibited TACE (PDB ID code 1bkc; the hydroxamate inhibitor, TapiII, was removed for clarity). The zinc ion (orange) is bound to His-405, His-409, His-415, and water as demonstrated by structural and spectroscopic studies (25). TACE's catalytic domain shares high sequence similarity with members of the matrix metalloproteinases (25, 26). (*b*) Pre-steady-state kinetics of QF45 hydrolysis by TACE. The reaction conditions were optimized by rapidly mixing 1.2 $\mu$M active TACE (catalytic domain, residues 215–473) and 4–20 $\mu$M QF45. Fluorescence emission from the product was monitored at >390 nm after excitation at 329 nm. The data (shown by open circles) consist of three main phases: lag phase, 0–34 ms, kinetic burst, 36–90 ms and steady-state phase, 90 ms, and on. Data were fitted (solid line) using a combination of a linear function and a single exponential equation, $F_{(t)} = a \times t + b + c \times e^{-kt}$, where $F_{(t)}$ is fluorescence intensity at a given time $t$ and reports on product formation, $a$ is the slope of the steady-state linear phase, $b$ is the offset value of this phase represented by the baseline height, $c$ is the amplitude of the exponential term, and $k$ is the apparent rate constant (s$^{-1}$). Under steady-state conditions (data not shown), the $k_{cat}$ and $K_m$ values were 232 $\pm$ 1.2 ms$^{-1}$ and 44.32 $\pm$ 7.2 $\mu$M, respectively.

of information cannot be addressed by kinetic analysis alone. Here we use this method to correlate the observed kinetic phases with the structure of transient zinc–protein intermediates and the local charge transitions that evolve during the initial peptide–protein interaction (lag phase) as well as during peptide hydrolysis (burst phase). This analysis provides direct experimental evidence for a peptide hydrolysis model that correlates the electronic transitions at the zinc site with defined catalytic steps.

For these experiments, we rapidly mixed and froze active TACE and substrate peptide in the stopped-flow freeze-quench apparatus. Sample mixtures were trapped during turnover in 5- to 10-ms time intervals over 5–233 ms (Figs. 1*b* and 2*a Inset*). On

the basis of our previous work (10), we expected that trapping enzyme–substrate complexes as they form during the early stages of catalytic turnover would increase the probability of trapping reaction intermediates. To probe the structure and electronics of the catalytic zinc–protein complex in TACE, frozen samples were probed with a monochromatic x-ray beam, and the x-ray absorption of the various time-dependent complexes were collected at the zinc K-edge.

### Probing the Structure of the Catalytic Zinc–Protein Complex in TACE

Fig. 2*a* (with the experimental set-up illustrated in the *Inset*) shows the fluorescence XAS data collected within the early stages of catalytic turnover using the time-resolved freeze-quench procedures. The data are presented in the form of Fourier transform (FT) spectra to provide the radial distribution of the various atoms within the first and second coordination shells of the catalytic zinc ion in TACE (the raw x-ray fluorescence data are presented *SI Text*). Apparent changes in the radial distribution spectra of the various time domains can be observed above the noise level. These spectral changes indicate that the local environment of the catalytic zinc ion undergoes structural transformations.

The shape and amplitude of the FT peaks are directly related to the type and number of the amino acid residues that are bound to the zinc ion. The first FT peak at time 0 corresponds to three Zn–N/O and one Zn–O/N atomic contributions and represent the coordination of the catalytic zinc ion to the three conserved histidine residues and water molecule at the enzyme active site (see also Fig. 1*a*) (5). Similarly, the second and third FT peaks (see arrows) are contributed by the atomic coordination of higher shells attributed by, for example, the alpha carbons of the histidine imidazole rings or the peptide backbone carbonyl. The observed deviations in both spatial distribution and peak intensities of the FT spectral features indicate unequivocally that the local structure of the catalytic zinc–protein complex is dynamically distorted during turnover.

The dynamic nature of the reaction mechanism of peptide binding to the catalytic zinc protein complex is evident in Fig. 2*a*. An abrupt increase in the first and second shell peak intensities of the FT spectra, at time scales corresponding to the reaction kinetic burst, indicate the direct coordination of the substrate peptide to the catalytic zinc ion (see blue arrow Fig. 2*a*). Remarkably, the process of the dissociation of the product from the catalytic zinc ion can be detected by the apparent restoration of the first FT peak intensity toward the resting active state and the shift of the second shell peak to higher distance (see red arrow) beyond the 88-ms time point at this level of data analysis. The shift of the second shell is seen before this time point and before reduction in first shell peak intensity. This finding may suggest that some conformational transitions are taking place in the enzyme active site before substrate dissociation.

Next we focused on precisely establishing the local structure around the catalytic zinc ion within TACE's active site by (*i*) obtaining the number of different intermediate species present at all time phases, (*ii*) identifying those species, and (*iii*) defining their relative abundance. For this, we applied a combination of principal component analysis, multiple data-set fits, and residual phase analysis (see *SI Text* for data-analysis strategy) (10, 12).

The coordination number, metal–ligand bond distances, and Debye–Waller factors of each time-dependent spectrum were refined by iteratively subtracting different fractions (from 0 to 90%) of the known steady-state XAS spectrum of substrate-free active TACE (i.e., the initial phase), followed by fitting of the residual spectrum to theoretical amplitudes and phases calculated via FEFF7, which is a program that calculates phase shifts and effective scattering amplitudes (13). During the kinetic burst phase, we detected the formation of a pentacovalent complex at
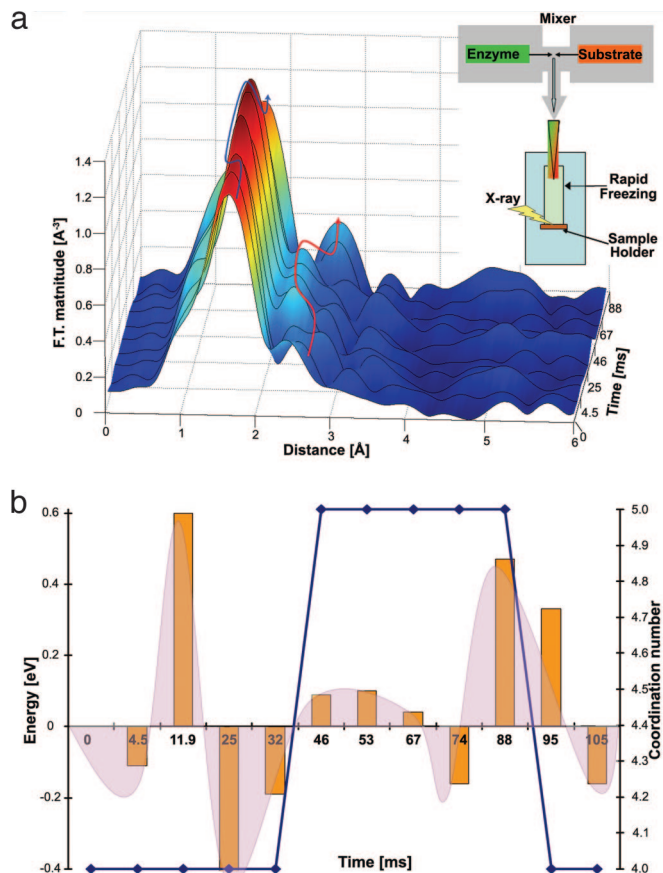
Solomon *et al.*

**Fig. 2.** Stopped-flow XAS analysis. (*a*) Magnitudes of the Fourier transform (FT) of $k^2$-weighted spectra, uncorrected for the photoelectron phase shifts ($\approx$0.5 Å), of the various time domains. The FT spectra were derived from the raw x-ray fluorescence data of the various time domains (before fitting analysis, see *SI Text* for details). Peak intensities above the noise level representing changes in the radial distribution of the atomic environment of the first, second, and higher atomic shells bound to the zinc atom within the TACE active site during catalysis. A comparison with the kinetic trace (Fig. 1*b*) shows no structural changes in the zinc–protein complex during the lag phase at time points 0–34 ms. An increase in first shell magnitude marked by the blue arrow (attributed to the formation of pentacoordinate zinc–protein complex at time point 46 ms) can be detected upon substrate binding to the zinc ion. In addition, an enhanced contribution of the second shell, Zn–C atomic distance, marked by a red arrow, is observed in synchronization with the increase in first shell peak intensity and the formation of the pentacoordinate intermediate (see Table 1). Finally, reduction in the first shell peak intensity (follow the blue arrow) and elongation of second shell Zn–C bond distance (follow the red arrow) is observed upon dissociation of the peptide substrate from the zinc ion due to product formation at 88 ms. (*Inset*) Illustration of the time-resolved freeze-quench XAS set-up. Reaction components (TACE and peptide substrate) are rapidly mixed (dead time = 2.1 ms), sprayed into a precooled isopentane bath, and collected inside a sample holder. Samples are exposed to a monochromated x-ray beam. Enzyme–substrate complexes formed at different reaction times are trapped and collected at appropriate times determined by monitoring the kinetics of the system by fluorescence emission spectroscopy. (*b*) The derivative of each time point of the absolute edge position during catalysis indicates the relative shift in edge energy (left *y* axis). Shifts in edge position are calculated with respect to the state of the sample at the start time of 0 ms. Changes in edge energy are correlated with the total effective charge of the zinc ion. Distinct charge transitions are detected during the kinetic lag phase (0–34 ms). Restoration of the zinc–protein charge transitions is observed at the end of the catalytic cycle approaching steady state (88–105 ms). The absolute position of the K-edge energy is indicative of the oxidation state of the absorbing atom (10). A shift to higher energy is associated with a more positive (more oxidized) effective charge on the metal ion. The change in the total coordination number of the zinc–protein complex (reported in

the catalytic zinc ion at 46 ms with a rather long lifetime ($\approx$40 ms). This stable intermediate evolved upon substrate binding to the catalytic zinc ion. After formation of substrate–enzyme complex, we observed the dissociation of the product from the catalytic pocket (complete dissociation observed after 88 ms), resulting in the formation of a tetrahedral complex at the zinc ion.

Table 1 summarizes the dynamic changes in atomic distances of the various zinc–protein–substrate ligands, including direct visualization of the binding of the peptide to the zinc ion and its dissociation after product release during a single catalytic turnover. This structural information is obtained from nonlinear fitting analysis of the experimental XAS spectra to the calculated XAS spectra (phase shifts and calculated scattering amplitudes) from the crystallographic coordinates of TACE and related matrix metalloproteinase structures (see *SI Text*). The observed dynamic changes in first shell bond distances are supported by concomitant changes in the second zinc ligand coordination shell (contributed by changes in Zn–C distances, see *SI Text*). Our attempts to detect intermediates at later reaction stages were inconclusive because of poor fits, due to the loss of synchronicity between the evolving intermediate states and their relatively low concentrations within this time frame.

The formation of pentacoordinated zinc–protein–substrate intermediates is indicated by the detection of additional Zn–O/N contribution. The local structure of this complex is assigned based on the described EXAFS analysis, and the identity of the fifth protein–substrate bond is rationalized based on the transient kinetic analysis. Specifically, this complex is detected only at the kinetic burst. Dissociation of the substrate from the catalytic zinc complex is observed by the elongation of the Zn–O/N bond distance as approaching steady state. The assignment of specific atomic contributions detected by our stopped-flow EXAFS analysis is supported by (*i*) crystallographic and spectroscopic structures of the resting state of TACE and (*ii*) the remarkable consistency between the distinct transient kinetic phases and the lifetime of the detected structural intermediate.

## Detection of Active Site Charge Transitions Upon Substrate Recognition and During Catalysis

Relative changes in the oxidation state of the zinc ion were analyzed by monitoring the shifts in edge energy of the raw XAS data (at the spectral edge region) among the different time-dependent XAS spectra along the peptide hydrolysis reaction. Changes in local charge and coordination number may be correlated with changes in spectral edge energy. This correlation is mostly significant for spectroscopically silent ions such as zinc. The inflection point of the spectral edge region was used for "edge energy" determination (see *SI Text*). Remarkably, significant changes in the total effective charge of the catalytic zinc ion are detected before the binding of the peptide substrate to the catalytic zinc ion and the formation of the pentacovalent complex. Importantly, these changes are detected during the kinetic lag phase (0–34 ms). Partial neutralization of this charge effect is observed during the kinetic burst, whereas the dissociation of

Table 1) is represented by the blue line (right *y* axis). The coordination number is determined by EXAFS analysis of the evolving reaction intermediates (see text and *SI Text*). The zinc ion preserves its tetrahedral coordination to three histidine residues and a water molecule during the kinetic lag phase at 0–34 ms. Formation of the pentacoordinate zinc–protein–substrate configuration (with an additional Zn–N/O contribution) in some TACE molecules in the sample is detected during the kinetic burst at 46–88 ms. Dissociation of the additional Zn–O/N bond is detected by restoration of the tetrahedral complex (at 95 ms) and elongation of the Zn–O/N bond (Table 1, at 74–88 ms). The effect of total charge transitions is represented by the integrated area under the orange bars.

**Table 1. Nonlinear curve fitting data analysis parameters of zinc–protein ligand intermediates during a single catalytic cycle of TACE**

| Time, ms | $\chi^2$ | $\Delta E_0$, cV | 3 × Zn–N/O I | | 1 × Zn–N/O II | | 1 × Zn–N/O III | |
|---|---|---|---|---|---|---|---|---|
| | | | R Å | $\sigma^2$, Å² | R, Å | $\sigma^2$, Å² | R, Å | $\sigma^2$, Å² |
| 0 | 0.22 | 6.8 | 2.11 ± 0.01 | 5.6E-03 ± 2E-03 | 1.95 ± 0.02 | 6.0E-03 ± 4.5E-03 | | |
| 4.5 | 0.96 | 7.8 | 2.14 ± 0.02 | 1.2E-03 ± 4.7E-04 | 1.94 ± 0.01 | 2.2E-03 ± 2E-03 | | |
| 11 | 1.26 | 5 | 2.10 ± 0.01 | 1.0E-06 ± 3E-04 | 1.95 ± 0.01 | 3.6E-03 ± 8E-04 | | |
| 25 | 7.58 | 8 | 2.13 (F) | 4.0E-04 ± 3E-03 | 1.90 ± 0.01 | 1.0E-06 ± 4E-03 | | |
| 32 | 1.17 | 6.4 | 2.11 ± 0.02 | 5.9E-03 ± 2E-03 | 1.98 ± 0.01 | 4.6E-03 ± 3E-03 | | |
| 46 | 3.48 | 4 | 2.13 ± 0.01 | 6.8E-05 ± 1E-03 | 1.94 ± 0.01 | 3.6E-04 ± 1E-03 | 1.94 ± 0.01 | 1.0E-06 ± 1E-03 |
| 53 | 4.03 | 6.9 | 2.18 (F) | 1.0E-02 ± 3E-03 | 2.03 ± 0.03 | 1.8E-03 ± 9E-03 | 1.97 ± 0.02 | 2.4E-03 ± 6E-03 |
| 67 | 0.10 | 7.5 | 2.20 ± 0.03 | 6.3E-03 ± 1E-03 | 1.99 ± 0.01 | 5E-03 (F) | 1.99 ± 0.01 | 4.3E-03 ± 1E-03 |
| 74 | 0.20 | 7.06 | 2.10 (F) | 1.6E-03 ± 7E-04 | 1.95 ± 0.03 | 1.0E-06 ± 5E-04 | 2.27 ± 0.02 | 5.6E-04 ± 2E-03 |
| 88 | 1.83 | 5.8 | 2.11 ± 0.03 | 6.7E-03 ± 2E-03 | 1.93 (F) | 5.0E-04 ± 2E-03 | 2.26 ± 0.03 | 4.8E-03 ± 5E-03 |
| 95 | 0.59 | 7 | 2.09 ± 0.01 | 3.6E-03 ± 1E-03 | 2.05 (F) | 1.0E-02 ± 5E-03 | | |
| 105 | 16.76 | 6 | 2.12 ± 0.02 | 1.7E-03 ± 3E-05 | 1.94 ± 0.03 | 1.0E-06 ± 3E-03 | | |

Detailed fits are shown in *SI Text*. The starting complex of TACE is represented at time 0, obtained by rapidly mixing and freeze-quenching TACE with buffer before introducing the substrate. The rest of the fits are of the residual spectra resulting from iterative subtractions of fractions of the starting phases (time 0). 3 × Zn–N/O I represents the average bond distance for three Zn-His residues. 1 × Zn–N/O II represents the bond distance contribution from N/O atom (water or peptide substrate). 1 × Zn–N/O III represents the bond distance contribution of the N/O atoms (water or peptide substrate). More than formation of pentacoordinate complex is detected at 46–88 ms. Elongation of the Zn–O III bond distance is detected, presumably during dissociation of the substrate from the catalytic zinc ion approaching steady state. $E_0$, the relative energy shifts used in the fits, R, Zn/ligand distance in Å; $\chi^2$, quality of the fits represented in $\chi^2$; $\sigma2$, thermodynamic disorder in Å; (F), parameters that were fixed in the fitting analysis.

the peptide substrate (starting at 88 ms) results in restoration of the observed charge flow transitions (see Fig. 2). These spectral shifts were reproducible and hence are not dependent on the freeze-quench process during sample preparations. Correlation between the time scales of the observed energy shifts and that of the observed kinetic phases indicates that the zinc ion is partially oxidized (as indicated by the high energy value at the 11.9-ms time point) and then partially reduced during the lag phase (at 25–32 ms), presumably upon interaction of the substrate with distal protein side chains because no local structural changes were detectable around the catalytic zinc complex during this phase (Fig. 2b and Table 1). Note that direct assignment of individual charge transitions to distinct chemical events throughout the catalytic reaction is limited at this stage of experiment. For example, the partial reduction of the zinc ion observed at 74 ms may result from a chemical or protein conformational process at higher coordination shells.

### Implications for Understanding Protease Reaction Mechanisms

Because of its great importance, the molecular mechanism of peptide hydrolysis is extensively studied. Theoretical analyses have suggested detailed reaction models, but until now, there has been only limited and controversial experimental evidence to support them.

Previous theoretical models for on carboxypeptidase A (CPA) argued that the zinc-coordinated water molecule is displaced by the peptide carbonyl oxygen and activated by a conserved active site Glu residue during peptide hydrolysis (Fig. 1a and *SI Text*). In this model, the zinc remains tetrahedrally coordinated throughout the reaction (4, 14). X-ray crystallography and kinetic studies of CPA, together with more advanced theoretical calculations, suggested a contradicting model in which the water molecule is bound to the zinc ion throughout its transformation to the hydroxyl ion. This process is then followed by the binding of the peptide carbonyl to the zinc ion to form a pentacovalent zinc–protein–substrate complex (3, 4). Our results provide real-time and direct evidence for the formation of the pentacoordinate catalytic zinc–protein complex during the peptide hydrolysis reaction as proposed by Lipscomb and coworkers (3). This intermediate has a relatively long lifetime, suggesting its key role in peptide hydrolysis reactions.

Remarkably, recent theoretical calculations on matrix metalloproteinase 3 predicted that dynamic changes in partial charges in the catalytic zinc–protein complex are taking place during the early stages of peptide hydrolysis while the peptide is directly coordinated to the zinc ion. The role of such changes was attributed to the mediation of the conversion of water to an hydroxyl ion required for nucleophilic attack and oxyanion formation occurring during peptide hydrolysis (6). This theoretical reaction model supports the notion that such local charge plasticity is mediated at the pentacovalent intermediate state, where the peptide carbonyl oxygen coordinates the zinc ion. Using our approach, we revealed experimentally that local charge transitions at the catalytic zinc–protein complex are indeed taking place even before the formation of the zinc–protein–substrate pentacoordinate intermediate.

Overall, we have performed an experiment aimed at measuring concomitant electronic and structural processes taking place inside the active site of a zinc–protein enzyme during catalysis. Using stopped-flow XAS at the zinc K-absorption edge, we were able to probe the structure and electronics of a catalytic ion that has, until now, been spectroscopically silent. Such direct characterization of real-time trapped reaction intermediates evolving during peptide hydrolysis of TACE enables us to refine the molecular mechanism suggested for such prototypical zinc–metalloproteinase enzymes.

Unexpectedly, we found that the reaction is governed by initial charge transitions of the catalytic zinc ion followed by dynamic structural transformations of the tetrahedral catalytic zinc–protein complex. This is mediated by the binding of the peptide substrate to the zinc ion forming pentacoordinate transient complex followed by product release and restoration of the tetrahedral zinc–protein complex.

Our results emphasize the importance of local charge transitions at the zinc ion before the formation of the pentacoordinate zinc intermediate in mediating effective catalysis. Importantly, this work indicates the presence of long range "communication pathways" between distal protein domains (such as substrate binding protein surfaces) and the catalytic machinery. Interestingly, the charge behavior of the zinc ion exhibits an oscillatory pattern. This may indicate that substrate interactions with the protein moiety induce discrete charge transitions required for
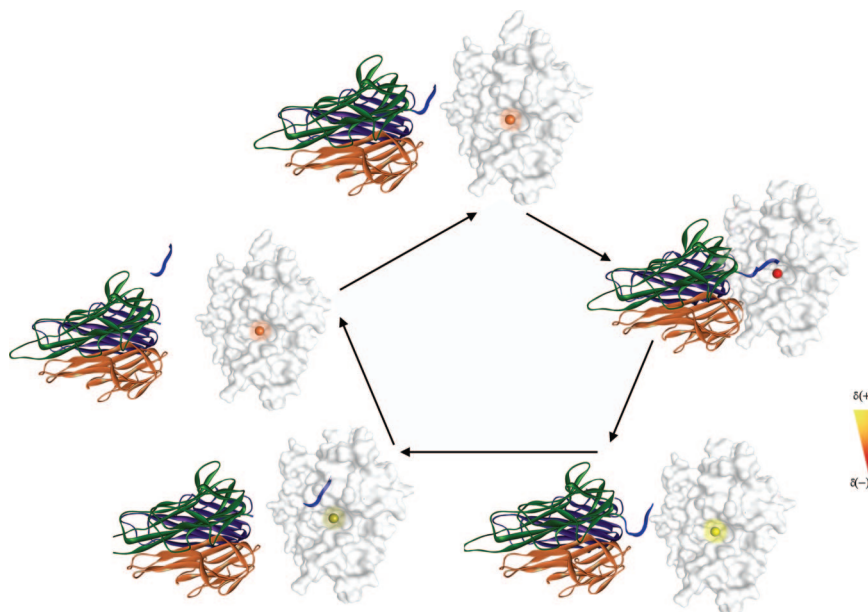
Solomon *et al.*

**Fig. 3.** Schematic model of how the TACE hydrolysis reaction might proceed with one of its substrates, pro-TNF-$\alpha$ (TNF-$\alpha$, PDB ID code 1tnf). The TACE catalytic domain (PDB ID code 1bkc) is rendered as a solid white surface; the catalytic zinc–protein complex environment is colored according to an artificial color scheme that represents the experimentally observed relative oxidation state of the zinc ion during catalysis (see Fig. 2b for relative values). Pro-TNF-$\alpha$ is rendered as solid ribbons, with each monomer colored differently. The peptide cleavage site has been drawn in schematic way. Molecules were rendered by using the Weblab viewer, and the images were processed by using Adobe Photoshop. In the enzyme's active state, the catalytic zinc ion is coordinated to three $\varepsilon$-N atoms from His-405, His-409, and His-415 and a water molecule. The reference point is the relative charge at the catalytic zinc ion in the TACE active site at 0 ms, before interaction with the substrate. Partial oxidation (not shown) followed by partial reduction (designated in yellow) of the catalytic zinc ion is detected upon interaction of TNF-$\alpha$ with TACE's protein surface. Substrate recognition, which presumably results in active site conformational changes, induces partial oxidation of the zinc ion, at the kinetic lag phase 0–34 ms, and the subsequent binding of Glu-406 to the zinc coordinated water molecule (see *SI Text* for molecular details). The catalytic hydroxyl ion is formed and charge is withdrawn by the metal ion from the hydroxyl group resulting in partial reduction of the zinc ion and stabilization of the hydroxyl species. This promotes the nucleophilic reaction and the binding of the peptide substrate to the zinc ion to form the pentacoordinated zinc complex during the kinetic burst phase at 46–88 ms. Cleaved TNF-$\alpha$ dissociates from the zinc ion upon substrate hydrolysis and product release. The total effective charge of the zinc ion is restored to the charge values of the resting state at 105 ms (for more detailed reaction model, see *SI Text*).

peptide hydrolysis. Interruption of this fine-tuned process may affect catalysis.

Fig. 3 provides a dynamic reaction model for peptide hydrolysis by TACE using pro-TNF-$\alpha$ as a substrate. *In vivo*, the release of TNF-$\alpha$ is mediated by TACE's cleavage of the macromolecule pro domain. Fig. 3 emphasizes the transmission of communication signals from distal protein domains to the catalytic zinc site during catalysis. Pro-TNF-$\alpha$ binds to TACE's protein surface during the kinetic lag phase. Binding of TNF-$\alpha$ results in partial oxidation followed by partial reduction of the zinc ion, without substantial rearrangement. Cleavage of the pro domain in Pro-TNF-$\alpha$ is mediated by direct binding to the catalytic zinc ion during the kinetic burst. The product dissociates from the catalytic zinc ion and is released from the enzyme pocket while restoring the charge of the catalytic zinc ion.

Overall, this experiment-based model provides for the first time solid evidence for the proposed theoretical model of the peptide hydrolysis mechanism (6, 15, 16) (for molecular details, see *SI Text*). In addition, our multidisciplinary experimental approach opens research pathways for direct mechanistic investigation of related as well as unrelated enzymes.

### Application to the Design of Drugs for TACE
Pathologies directly related to TACE's proteolytic function include septic and toxic shock syndromes (17), transplant rejection (18), Crohn's disease (19), Alzheimer's disease (20), multiple sclerosis (21, 22), and several types of blood cell cancers (23). TACE's shedding of diverse, unrelated proteins of the secretory pathway with divergent cleavage sites underlines the complexity of substrate recognition and catalysis for this enzyme

(24). Almost 10 years after the identification of this protease and cloning of its gene, the molecular mechanisms controlling its activation, substrate recognition, and catalysis remain elusive.

Here we reveal that substrate recognition by TACE is accompanied by dynamic changes of the total effective charge of the zinc ion residing at the catalytic core of the enzyme, whereas the tetrahedral zinc complex remains intact. Presumably, this "charge plasticity" is mediated by protein conformational transitions and is required for the maturation of the zinc site for substrate catalysis. Interfering with such, presumably fine or subtle, conformation transitions may increase (or lower) the energy barrier required for catalysis; this suggests that selective inhibitors for TACE may be developed by targeting alternative sites different from the catalytic zinc site, in a way that blocks or critically perturbs the precursor electronic activity of the catalytic core in TACE. This approach departs from traditional drug design strategies used for metalloenzymes targeting the catalytic metal site with potent zinc chelating peptidomimetic compounds. This inhibition approach is based on the reported dynamic structural and electronic model of TACE during substrate hydrolysis but may be generalized to other related systems.

### Materials and Methods
**Materials.** The catalytic domain of human TACE was expressed and purified by using reported protocols (23). Fluorogenic peptide QF-45 [Mca-Ser-Pro-Leu-Ala-Gln-Ala-Val-Arg-Ser-Ser-Ser-Arg-Lys(Dnp)-NH$_2$] was synthesized at the Weizmann Institute core facilities.

**Steady-State Kinetic.** The enzymatic activity of TACE was measured at 37°C by monitoring the increased fluorescence intensity

upon degradation of the fluorogenic peptides, QF-45, at $\lambda_{ex} =$ 340 nm and $\lambda_{em} = 390$ nm. The standard assay mixture contained 50 mM Tricine buffer, pH 7.5, 100 mM NaCl, 10 mM $CaCl_2$, and 20% glycerol.

**Pre-Steady-State Kinetic Studies.** An Applied Photophysics (Leatherhead, U.K.) SX18 stopped-flow apparatus was used for transient kinetic studies. Time-resolved kinetic assays were conducted by using an excess of substrate (see *SI Text* for details).

**Stopped-Flow Freeze-Quench XAS.** A final concentration of 0.4 mM (11 mg/ml) TACE and nonfluoregenic QF-45 were rapidly mixed at 1:10 TACE:QF-45 ratio and froze BioKine SFM-300 freeze-quench module (SFM-300; Bio-Logic–Science Instruments, Claix, France). Time points of freezing were chosen in the single catalytic cycle (0–233 ms). Frozen samples were kept in liquid nitrogen at 30°K before exposure to x-rays.

**XAS Measurements and Analysis.** XAS data collection was performed at the National Synchrotron Light Source (NSLS), Brookhaven National Laboratory, beam-line X9B. Spectra were recorded at the zinc K-edge in fluorescence geometry at 30°K (see details in *SI Text*). Data were subjected to deconvolution data-analysis procedures and iterative subtractions following our reported procedures (10) (see also *SI Text* for detailed description of the data-analysis procedures).

1. Bode W, Fernandez-Catalan C, Tschesche H, Grams F, Nagase H, Maskos K (1999) *Cell Mol Life Sci* 55:639–652.
2. Brinckerhoff CE, Matrisian LM (2002) *Nat Rev Mol Cell Biol* 3:207–214.
3. Christianson DW, Lipscomb WN (1989) *Acc Chem Res* 22:62–69.
4. Kilshtain-Vardi A, Shoham G, Goldblum A (2002) *Int J Quantum Chem* 88:87–98.
5. Kotra LP, Cross JB, Shimura Y, Fridman R, Schlegel HB, Mobashery S (2001) *J Am Chem Soc* 123:3108–3113.
6. Pelmenschikov V, Siegbahn PE (2002) *Inorg Chem* 41:5659–5666.
7. Blobel CP (2005) *Nat Rev Mol Cell Biol* 6:32–43.
8. Amour A, Slocombe PM, Webster A, Butler M, Knight CG, Smith BJ, Stephens PE, Shelley C, Hutton M, Knauper V, *et al.* (1998) *FEBS Lett* 435:39–44.
9. Johnson KA (1992) *Enzymes* 20:1–61.
10. Kleifeld O, Frenkel A, Martin JM, Sagi I (2003) *Nat Struct Biol* 10:98–103.
11. Strange RW, Hasnain SS (2005) *Methods Mol Biol* 305:167–196.
12. Frenkel A, Kleifeld O, Wasserman SR, Sagi I (2002) *J Chem Phys* 116:9449–9456.
13. Rehr JJ, De leon JM, Zabinsky SI, Albers RC (1991) *J Am Chem Soc* 113:5135–5140.
14. Mock WL, Zhang JZ (1991) *J Biol Chem* 266:6393–6400.
15. Fersht A (1999) in *Structure and Mechanisms in Protein Science* (Freedman, New York), Vol 1, pp 472–491.
16. Antonczak SM, G. Lopez, MR. Rivail JL (2000) *J Mol Model* 7–8:527–538.
17. Dinarello CA (1991) *J Infect Dis* 163:1177–1184.
18. Elliott MJ, Maini RN, Feldmann M, Kalden JR, Antoni C, Smolen JS, Leeb B, Breedveld FC, Macfarlane JD, Bijl H, *et al.* (1994) *Lancet* 344:1105–1110.
19. Van Dullemen HM, Van Deventer SJ, Hommes DW, Bijl HA, Jansen J, Tytgat GN, Woody J (1995) *Gastroenterology* 109:129–135.
20. Allinson TM, Parkin ET, Turner AJ, Hooper NM (2003) *J Neurosci Res* 74:342–352.
21. Kieseier BC, Pischel H, Neuen-Jacob E, Tourtellotte WW, Hartung HP (2003) *Glia* 42:398–405.
22. Brosnan CF, Selmaj K, Raine CS (1988) *J Neuroimmunol* 18:87–94.
23. Jones PH, Christodoulos K, Dobbs N, Thavasu P, Balkwill F, Blann AD, Caine GJ, Kumar S, Kakkar AJ, Gompertz N, *et al.* (2004) *Br J Cancer* 91:30–36.
24. Milla ME, Leesnitzer MA, Moss ML, Clay WC, Carter HL, Miller AB, Su JL, Lambert MH, Willard DH, Sheeley DM, *et al.* (1999) *J Biol Chem* 274:30563–70.
25. Solomon A, Rosenblum G, Gonzales PE, Leonard JD, Mobashery S, Milla ME, Sagi I (2004) *J Biol Chem* 279:31646–54.
26. Massova I, Kotra LP, Fridman R, Mobashery S (1998) *FASEB J* 12:1075–1095.